Article

A Label-Free Colorimetric Assay Based on Gold Nanoparticles for the Detection of H_2O_2 and Glucose

Cong Zheng [1,†], **Da Wu** [1,†], **Tao Wang** [2], **Jianhong Xiao** [2] **and Li Yu** [1,*]

1   Key Laboratory of Colloid and Interface Chemistry, Shandong University, Ministry of Education, Jinan 250100, China; cc15275411396@163.com (C.Z.); 202032394@mail.sdu.edu.cn (D.W.)
2   Petroleum Engineering Technology Research Institute of Shengli Oilfield, Sinopec, Dongying 257000, China; wangtao202.slyt@sinopec.com (T.W.); xiaojianhong.slyt@sinopec.com (J.X.)
*   Correspondence: ylmlt@sdu.edu.cn; Tel.: +86-531-88364807; Fax: +86-531-88564750
†   These authors contributed equally to this work.

Abstract: The significance of sensing hydrogen peroxide (H_2O_2) is due to its ubiquity, being a potential biomarker as well as an end-product of several oxidation reactions. Herein, based on gold nanoparticles (AuNPs) and coupled with single-stranded DNA (ssDNA) and ceria nanoparticles (CeO_2), we developed a novel colorimetric method to detect H_2O_2 and glucose in NaCl solutions. In the presence of H_2O_2, ssDNA adsorbed on the surface of CeO_2 could be released and subsequently decorated AuNPs, resulting in a distinct color change of the aqueous solution from purple to red, which could be observed by the naked eye. Since H_2O_2 can be produced in the process of glucose oxidation by glucose oxidase (GOx), this approach can also be employed to detect glucose. By employing this sensing system, the detection limits for H_2O_2 and glucose are about 0.21 μM and 3.01 μM, respectively. Additionally, monitoring the content of glucose in blood serum samples was successfully achieved by the proposed strategy. This work opens a potential avenue for the quantitative detection of H_2O_2 and glucose in clinical diagnostics.

Keywords: gold nanoparticles; ceria nanoparticles; hydrogen peroxide; glucose; colorimetric assay

1. Introduction

The detection of physiologically important species plays a pivotal role in clinical diagnosis and medical research. H_2O_2, as a crucial biomarker, is of practical significance in chemical, biological, and clinical fields [1–3]. In addition, H_2O_2 is the final product in oxidation reactions and is catalyzed by glucose oxidase (GOx), cholesterol oxidase, and lactate oxidase, etc. [4,5]. It is essential to maintain the normal level of H_2O_2 for various biological processes and the assessment of human health hazards. An excess of H_2O_2 can induce various kinds of neurodegenerative diseases and biological damages in the human body; thus, accurate and rapid detections of H_2O_2 are necessary to prevent further impacts on human health. Currently, although a number of existing methods such as PtPd-Fe_3O_4 nanoparticles [6], boric-acid-functional [7], enzyme mimetics [8], hollow and porous Fe_3C-NC nanoballoons (Fe_3C-NC-NBs) [9], which are based on electrochemical approaches or fluorescence methods, have accomplished this goal, however, there are still challenges to develop neoteric techniques more adaptable to reliably detect H_2O_2, which do not rely upon advanced instruments and elaborately designed labels.

In recent years, nanomaterials have gained much attention in colorimetric biosensing and diagnostics on account of their unique physical or chemical properties [10–17]. Some nanomaterials such as graphene quantum dots (GQDs)/AgNPs hybrids and Pt nanoclusters [5,18] have been synthesized for the colorimetric detection of H_2O_2, but they generally require complex synthesis procedures or time-consuming operations. By comparison, AuNPs can be easily fabricated. It also possesses the ability to absorb ssDNA [10,19–22].

Moreover, it has a large surface-to-volume ratio and high extinction coefficient. Therefore, they have attracted extensive attention in colorimetric biosensors and diagnostics. In the past decades, a variety of AuNPs-based colorimetric assays for H_2O_2 has been developed [23,24]. However, many of these methods lack sufficient sensitivity and simple operation. Thus, making great efforts in seeking a novel approach for H_2O_2 monitoring is indispensable.

CeO$_2$, as one of the most reactive rare earth materials, possesses many attractive properties that make it highly promising for special applications in photocatalysis, conversion catalysts, three-way catalysts (TWCs), solar cells, gates for metal-oxide semiconductor devices and phosphors, and colorimetric sensors [25–31]. Moreover, due to a great affinity of CeO$_2$ for H_2O_2, it may be considered for use in H_2O_2 sensing systems with high sensitivity and selectivity [32].

As previously mentioned, H_2O_2 is a product of glucose oxidation; thus, generally, the assays that monitor H_2O_2 can be utilized for glucose detection. On the other hand, blood glucose concentration is the main basis for diabetes diagnosis, and it is also the main index of the patient's condition and degree of diabetes. For this reason, the detection of glucose is of great significance, resulting in the development of a variety of methods for the detection of glucose, such as mass spectrometry [33], electrochemistry [34–36], fluorescence [37,38], and colorimetric methods over the years. Among all of these methods, colorimetric methods have been investigated extensively due to their benefits such as simplicity, fast analysis speed, relatively low cost, sensitivity, and selectivity. Therefore, we developed a novel colorimetric method to detect H_2O_2 and glucose based on AuNPs, ssDNA, and CeO$_2$.

In the current study, we investigated interactions between H_2O_2 and CeO$_2$, combined with ssDNA and AuNPs in a high salt solution (Scheme 1). As illustrated in Scheme 1a, initially, ssDNA adsorbs on the surface of CeO$_2$ [32,39] when the ssDNA solution is mixed with a CeO$_2$ solution. Thereafter, in the addition of AuNPs solution and high concentration salt solutions, the aggregation of AuNPs occurs [40] due to there being no protection of ssDNA (presenting the macroscopical purple color. Upon the introduction of target H_2O_2, it induces ssDNA desorption from CeO$_2$ and binds to the surface of AuNPs, resulting in disaggregation and color change [24,41]. Hence ssDNA-decorated AuNPs can be finely dispersed (Scheme 1b), corresponding to the red color solution. When adding GOx, it is possible to monitor glucose even in blood serum samples. Thus, H_2O_2 and glucose can be easily detected using the colorimetric method via the observation of remarkable color change, and their detection limits can reach 0.21 μM and 3.01 μM, respectively. Due to the use of biocompatible AuNPs and nonpolluting CeO$_2$, the proposed strategy is relatively environmentally friendly. Moreover, it highlights a very promising strategy for the design of a new cost-effective and label-free family of H_2O_2 and glucose colorimetric sensors.

Scheme 1. Schematic illustration of AuNPs from aggregation (**a**) to dispersion (**b**) in the absence or presence of H_2O_2, respectively.

2. Materials and Methods

2.1. Materials

Chloroauric acid hydrated (HAuCl$_4$·3H$_2$O) was obtained from Sahn chemical technology (Shanghai, China) Co., Ltd. of China. Carboxyfluorescein (FAM)-labeled ssDNA (5' to 3' FAM-AGAAAAAACTTCGTGC) and ssDNAs with a random sequence (CAG GAT CAT GGT GAT GCT CTA CG) were purchased from Sangon Biotech Co., Ltd., Shanghai, China. 4-(2-hydroxyethyl)-piperazine-1-ethane sulfonic acid (HEPES, pH = 7.0) was purchased from Shanghai Yuanye Biotechnology Co., Ltd. Shanghai, China. GOx ($\geq$155,000 units/g, aspergillus niger) was supplied by Sigma-Aldrich. Glucose, CeO$_2$ nanoparticle suspension (conveniently shorted to CeO$_2$, particle size 10~20 nm), fructose, ascorbic acid, dopamine, cysteine, alanine, galactose, and sucrose were commercially available from J&K Scientific Co., Ltd., China. Hydrogen peroxide (H$_2$O$_2$, $\geq$30.0%), KCl, ZnCl$_2$, NaCl ($\geq$99.5%), and trisodium citrate ($\geq$99.0%) were procured from Sinopharm Chemical Reagent Co., Ltd., Beijing, China. All chemicals were used without further purification. Ultrapure water was used in experiments. ssDNA, FAM-labeled ssDNA, and GOx were diluted in HEPES buffer, respectively. The other chemicals were dissolved in water.

2.2. Instruments

UV-vis absorption spectra of samples were measured by a Cary-5000 UV-vis spectrometer (Agilent) in a quartz cell (light path of 5 mm). The water signal, as the background signal, was taken away from the sample signal. Transmission electron microscopy (TEM) images were obtained by an HT-7700 instrument. The accelerating voltage was 120 kV. The particle size distribution diagram was obtained by Laser Particle Size and a Zeta Potential Analyzer. A FluoroMax-4 fluorescence spectrophotometer was used to determine the fluorescence spectra of samples. Under the condition of excitation at 490 nm with an Xe lamp, the fluorescence signals were recorded in the range of 505~640 nm. Slits for both excitation and emission measurements were 1.2 nm.

2.3. Preparation Procedures of AuNPs

AuNPs were fabricated by using trisodium citrate reductions in HAuCl$_4$, following the procedures reported earlier [42–44]:

(1) Ultrapure water (98 mL) and 50 mM HAuCl$_4$ (2 mL) were mixed in a three-neck flask and then heated to boil under stirring.
(2) An amount of 38.8 mM trisodium citrate (10 mL) was transferred into the above flask rapidly. The mixture was heated in the condition of reflux with vigorous stirring for 15 min. During this process, the color of the solution changed from pale yellow to deep red gradually, which indicates the formation of AuNPs.
(3) Centrifuge the solution for 15 min at a speed of 8000 r/min. The as-prepared AuNPs were redispersed with ultrapure water and stored at 4 °C for later use.

2.4. Detection Assays of H$_2$O$_2$ and Glucose

The process for H$_2$O$_2$ detection was carried out as described below: ssDNA (200 μL, 1 μM) was firstly mixed with CeO$_2$ (200 μL, 200 mg/mL). Then, 200 μL of H$_2$O$_2$ solution (0.1, 1×10^{-3}, 1×10^{-4}, 1×10^{-6}, 1×10^{-7} and 1×10^{-8} M) was introduced to the above-mentioned mixture. After that, AuNPs (200 μL, 17 nM) were slowly added in 1 min, followed by introducing NaCl (200 μL, 0.2 M) over the course of 1 min at room temperature. The absorption spectra ranging from 350 to 700 nm was measured by a spectrophotometer.

For the detection of glucose, the details were as followed: 100 μL of glucose solution with various concentrations (5, 0.5, 0.1, 0.05, 0.01, and 0.001 mM) was separately cultivated with GOx (100 μL, 0.05 mg/mL) at 37 °C for 40 min, which was subsequently introduced into the mixture of ssDNA and CeO$_2$. Then, AuNPs (200 μL, 17 nM) and NaCl (200 μL, 0.2 M) solutions were successively added to the above solution. Finally, the resulting mixture was applied to spectroscopic measurements. In addition, 0.01 mM glucose was

replaced by sucrose, galactose, and fructose with the same concentration to verify the specificity of this strategy.

2.5. Detection of Glucose in Diluted Serum Samples

The blood samples, collected from healthy adults (provided by a local hospital), were firstly centrifuged at 8000 r/min for 10 min to remove large aggregates and then diluted 500 times with HEPES buffer (pH = 7, 10 mM) without any other treatment before further experiments. HEPES (pKa at 20 °C: 7.45–7.65) is a zwitterionic, piperazinic buffer that is useful for a pH range of 6.8–8.2. In order to detect the content of glucose in diluted serum samples, the standard addition method was used [45]. Firstly, diluted serum (10 μL) and glucose solution (10 μL) with different concentrations were added into HEPES (80 μL) buffer. Then, the samples were utilized to detect glucose according to the same steps as mentioned above.

3. Results and Discussion

3.1. Characterizations of AuNPs and CeO_2

AuNPs fabricated by the trisodium citrate reaction method have an average diameter of ~13 nm [42] (Figure 1a) and their solution displayed a distinct wine-red color with a distinctive absorption peak at approximately 523 nm (Figure 1b). Therefore, the concentration of the AuNPs solution was evaluated to be about 17 nM according to the Lambert–Beer law with an extinction coefficient of 2.78×10^8 $M^{-1} \cdot cm^{-1}$ for 13 nm AuNPs [46]. Some information on the size and morphology of CeO_2 can be obtained from Figure 2. TEM images indicate that CeO_2 was dispersed relatively well (Figure 2a). The size distribution determined by DLS illustrates that the average diameter of CeO_2 is ~20 nm (Figure 2b).
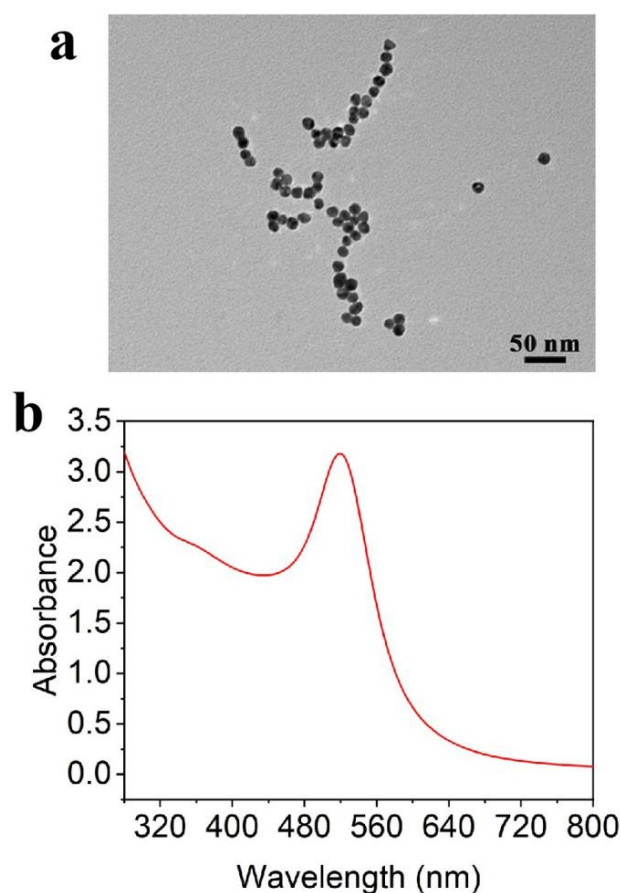
Figure 1. TEM image (**a**) and UV−vis absorption spectrum (**b**) of the synthesized AuNPs.
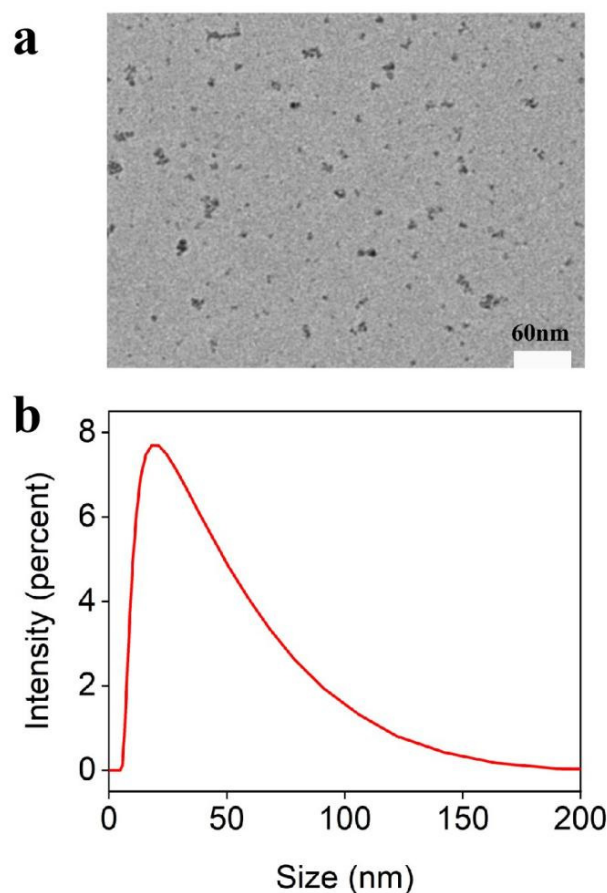
Figure 2. TEM image (**a**) and DLS (**b**) of the nano$-CeO_2$ sample used in this work.

3.2. Mechanism of the Visual Assay for H_2O_2

In ordre to investigate the feasibility of the visual method for H_2O_2 sensing, AuNPs were used as a colorimetric substrate because of their low cost, nontoxicity, and ease of unaided visual detection. As observed from Figure 3a(I), the intensity of absorbance spectrum of the (ssDNA + CeO_2 + AuNPs + NaCl) system at about 523 nm is clearly reduced, and a new peak emerges at around 625 nm. While adding H_2O_2, there only exists a strong absorption peak at 523 nm (Figure 3a(II)). Concomitantly, the color of the mixed solution changes from purple to red in the case of H_2O_2 (Figure 3a). Thus, in the presence of H_2O_2 and high concentration salt solution, the adsorption of ssDNA on the surface of AuNPs will cause good dispersion of AuNPs along with red color solution. These data demonstrate the possibility of using (ssDNA + CeO_2) to directly detect H_2O_2 using AuNPs in high concentration salt solutions.

To elucidate the mechanism of this sensing system for H_2O_2, FAM-labeled ssDNA was employed to determine the fluorescence spectrum. As shown in Figure 3b, it exhibits a distinct emission peak at ~520 nm. Furthermore, the fluorescence of FAM-ssDNA was quenched obviously upon the introduction of CeO_2, which may be due to adsorption of FAM-ssDNA. Significant fluorescence recovery was observed after adding H_2O_2. Since it was demonstrated by a previous study that H_2O_2 binds to CeO_2 more strongly than FAM-ssDNA [32], we speculate that, in the presence of H_2O_2, FAM-ssDNA is desorbed from the surface of CeO_2 and released to the aqueous solution. Interestingly, when adding AuNPs into the mixed solution mentioned above, fluorescence quenching occurred immediately as a result of FAM-ssDNA adsorption on the surface of AuNPs [47].
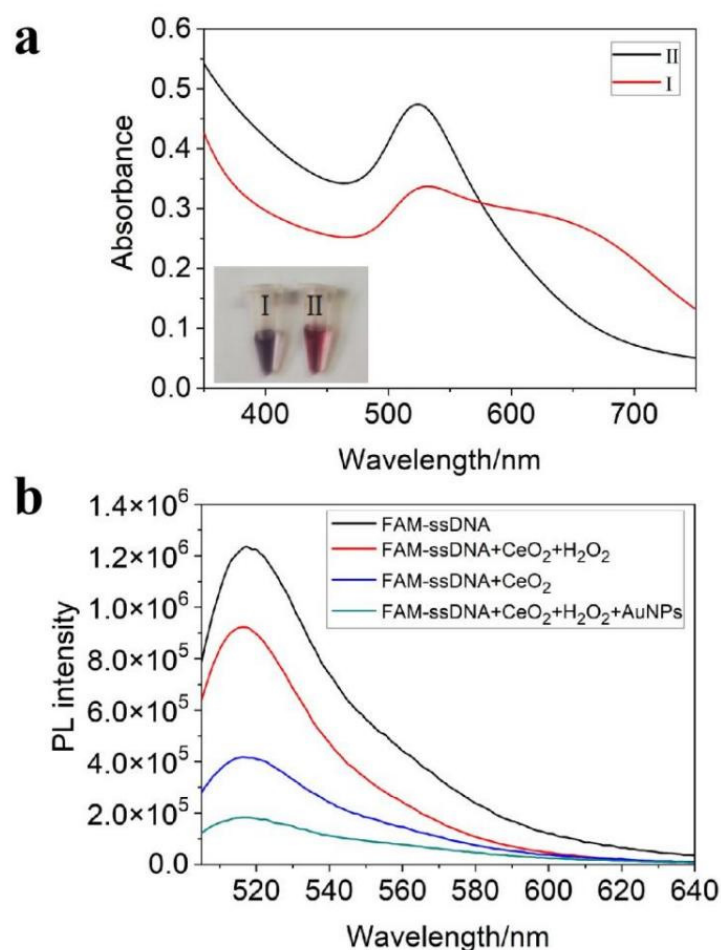
Figure 3. (**a**) UV−vis absorption spectra of (I) ssDNA + CeO_2 + AuNPs + NaCl and (II) H_2O_2 + ssDNA + CeO_2 + AuNPs + NaCl (the inset, corresponding optical photographs). (**b**) Fluorescence spectra of different systems. (The concentrations of CeO_2, ssDNA, FAM−ssDNA, H_2O_2, AuNPs, and NaCl were 200 μg/mL, 1 μM, 1 μM, 0.1 M, 17 nM, and 0.2 M, respectively.)

3.3. Optimal Doses of ssDNA and CeO_2 for the Assay

Previous studies have proven that AuNPs decorated with ssDNA can be finely dispersed when 0.2 M NaCl is introduced [20]. It is necessary to investigate the optimum concentration of ssDNA solution required to be adsorbed on the surface of AuNPs in NaCl aqueous solution. In Figure 4a,b, the stability of AuNPs was investigated over ssDNA concentration gradient within the range of 0.2~1.0 μM in the presence of 17 nM AuNPs and 0.2 M NaCl. With the increasing concentration of ssDNA, a visual color of mixed solution changed from purple to red (Figure 4a) and a descent in the UV-vis absorption intensity at 523 nm were observed. When the concentration of ssDNA increased to 1.0 μM, the color and UV-vis spectrum of the mixed solution were almost similar to those of the AuNP solutions. Thus, 1.0 μM of ssDNA was employed to carry out the subsequent experiments.

The effect of (ssDNA + CeO_2) on the existence state of AuNPs in 0.2 M NaCl solution was explored in the concentration range of 50~200 μg/mL CeO_2. As shown in Figure 5a, when the concentration of CeO_2 increased to 200 μg/mL, the color of mixed solution transformed from red to purple. As observed in Figure 5b, compared to the absorption spectra of a relatively low concentration of CeO_2, for 200 μg/mL CeO_2, a new peak emerges at around 625 nm. These results suggest that AuNPs aggregation could occur in (ssDNA + CeO_2 + NaCl) system as CeO_2 was modified by ssDNA due to the coordination interaction between the ssDNA backbone and CeO_2 [48]. Based on this, 1.0 μM ssDNA and 0.2 M NaCl with a fixed concentration of CeO_2 (namely 200 μg/mL) can be utilized for the following experiments.
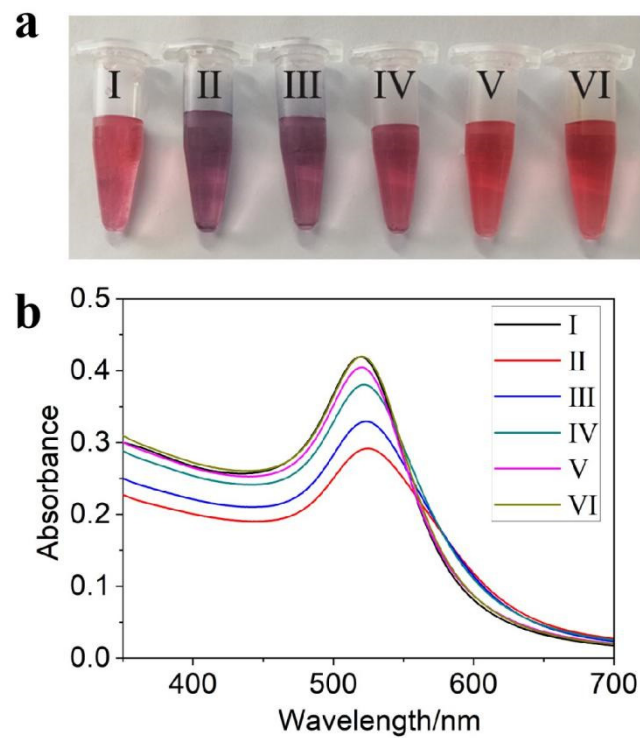
Figure 4. (**a**) Visual color changes of AuNPs (I) and (AuNPs + NaCl) in different concentrations of ssDNA: (II) 0.2 μM, (III) 0.4 μM, (IV) 0.6 μM, (V) 0.8 μM, and (VI) 1.0 μM. (**b**) UV−vis absorption spectra corresponding with samples in (**a**).
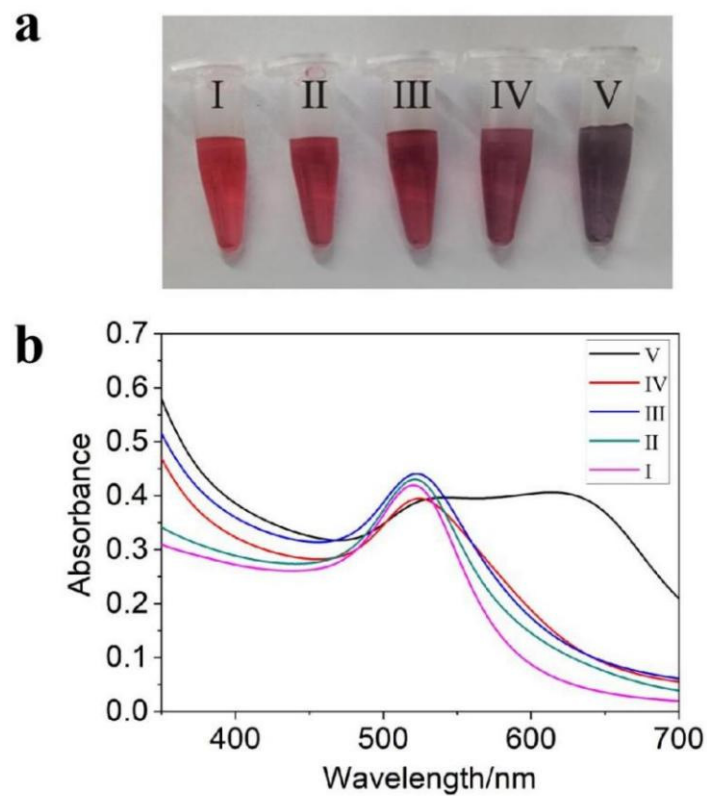

Figure 5. (**a**) The color changes and (**b**) UV−vis absorption spectra of (AuNPs + ssDNA + NaCl) in different concentrations of CeO₂: (I) 0, (II) 50 μg/mL, (III) 100 μg/mL, (IV) 150 μg/mL, and (V) 200 μg/mL.

3.4. Colorimetric Detection of H_2O_2 and Glucose Using the Assay

According to the above results, we proposed a label-free and colorimetric method to monitor H_2O_2. In the presence of different concentrations of H_2O_2, the concentration-dependent color changes and the corresponding absorption spectra are exhibited in Figure 6a,b, respectively. The visual color of solutions undergoes a red-to-purple transformation, accompanied by an increased absorption at 523 nm (A_{523}) and a decreased absorption at 625 nm (A_{625}) with increasing concentrations of H_2O_2. Additionally, as observed from Figure 6c, the ratio of A_{625}/A_{523} shows a linear relationship (the linear relationship is $Y = 0.3242 - 0.0538X$, correlation coefficient of $R^2 = 0.991$) within the H_2O_2 concentration range of 1×10^{-8}~0.1 M. The limit of detection (LOD) of H_2O_2 was calculated, using standard methods (LOD = 3 S/slope), to be 0.21 μM. S is the standard deviation of the blank sample. The slope was obtained from the standard curve (Figure 6c). As illustrated in Table 1, the linear range of our strategy for H_2O_2 detection is wider than that of the current methods. Moreover, the correlation coefficient of the linear equation for this method is higher than that of some reported approaches. Moreover, the sensitivity of our strategy is better than most of the current methods (Table 1). Although the LODs of nanostructured polysaccharide (cellulose nanowhiskers) CNW-AgNPs film [49], GQDs-AgNPs film [50], and Eu-MOF film [35] are lower than this work, there exist some aspects to improve. For example, the synthesis procedures of CNW and Eu-MOF are complex and the GQDs-AgNPs film contains AgNPs, which has higher biological toxicity. Therefore, the strategy proposed in this work has some obvious advantages to detect H_2O_2.
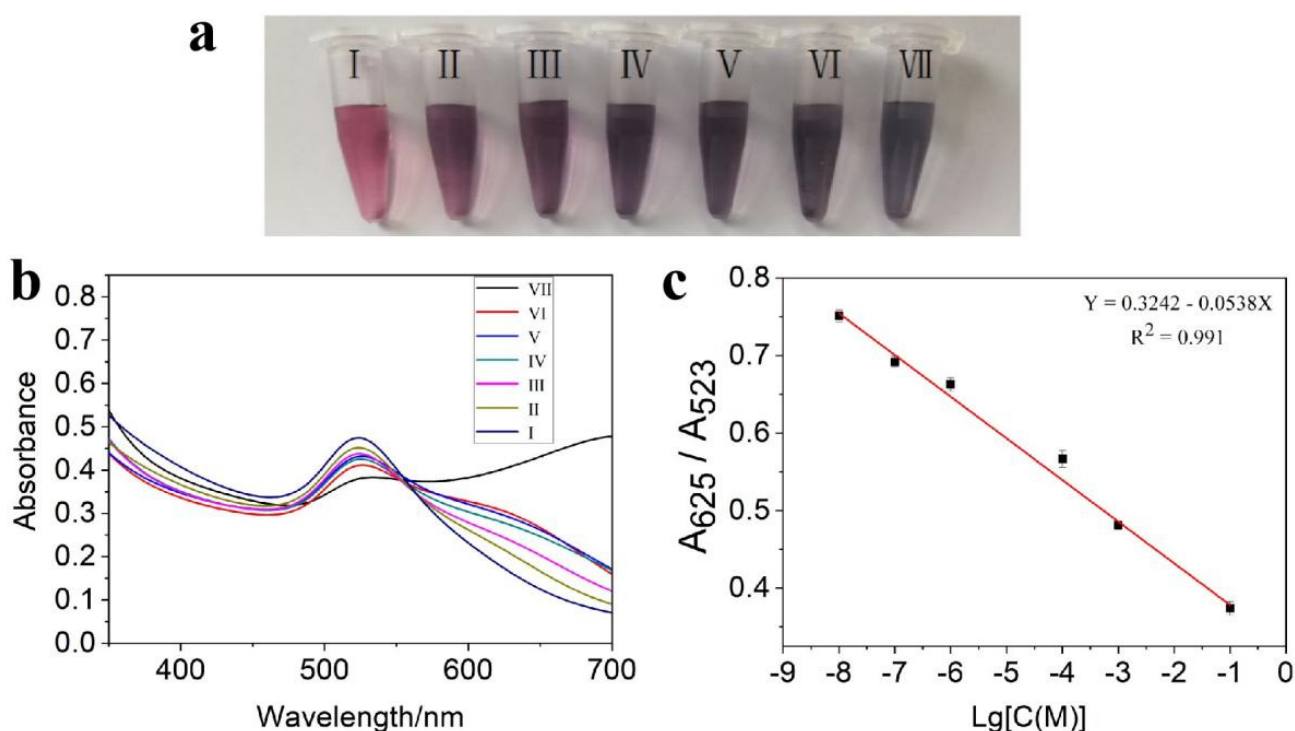

Figure 6. (**a**) Visual color changes of CeO_2 + ssDNA + AuNPs + NaCl in the presence of different concentrations of H_2O_2: (I) 0.1 M, (II) 1×10^{-3} M, (III) 1×10^{-4} M, (IV) 1×10^{-6} M, (V) 1×10^{-7} M, (VI) 1×10^{-8} M, and (VII) 0 M. (**b**) UV−vis absorption spectra change corresponding with (**a**). (**c**) The linear fitted curve presenting the A_{625}/A_{523} absorbance ratio at different concentrations of H_2O_2; error bars indicate S (*n* = 3).

Table 1. Comparison of this work with other methods for H_2O_2 detection.

Detection Type	Linear Relationship	Linear Range/μM	LOD/μM	Reference
Nanostructured polysaccharide-AgNPs	$Y = 0.6632 - 0.052X$ ($R^2 = 0.9801$)	0.01–30	0.014	[49]
GQDs-AgNPs	$Y = 1734 X + 2.74412$ ($R^2 = 0.98615$)	0.5–50	0.162	[50]
TiO$_2$-cytochrome c	-	0.85–24,000	0.26	[51]
PtPd-mesoporous carbon	-	0.5–27,000	0.30	[52]
HRP-CNT-chitsan-sol-gel	$I^{-1} = 0.03454 + 0.22497C^{-1}$ ($R^2 = 0.9970$)	-	1.40	[53]
HRP-Au-chitosan-clay	$I^{-1} = -0.06955 + 1.6098C^{-1}$ ($R^2 = 0.9964$)	39–3100	9.00	[54]
Pt-MnO-graphene	-	2.0–13,330	5.00	[55]
Eu-MOF	$Y = 3.1823 + 0.0732X$ ($R^2 = 0.9815$)	0.05–2	0.0335	[35]
AuNPs	$Y = 0.3242 - 0.0538X$ ($R^2 = 0.991$)	0.01–100,000	0.21	This work

Glucose could be oxidized to produce H_2O_2 and gluconic acid after the reaction of GOx and O_2. Thus, this H_2O_2 sensing assay was further used to monitor glucose. The results of glucose detection are presented in Figure 7a. As shown, visual color changes (red color to purple color) were observed with an increase in the content of glucose (0~5 mM). The corresponding UV-vis absorption spectra were determined and displayed in Figure 7b. As presented in Figure 7c, the A_{625}/A_{523} value decreases linearly (the linear relationship is $Y = 0.6319 - 0.0984X$, $R^2 = 0.995$) with the logarithm of glucose concentration (0.001~5 mM), based on which the LOD for glucose is estimated to be around 3.01 μM. In contrast, the correlation coefficient of the linear equation and the detection sensitivity of this assay is predominant over most other glucose-responsive detective methods (Table 2).
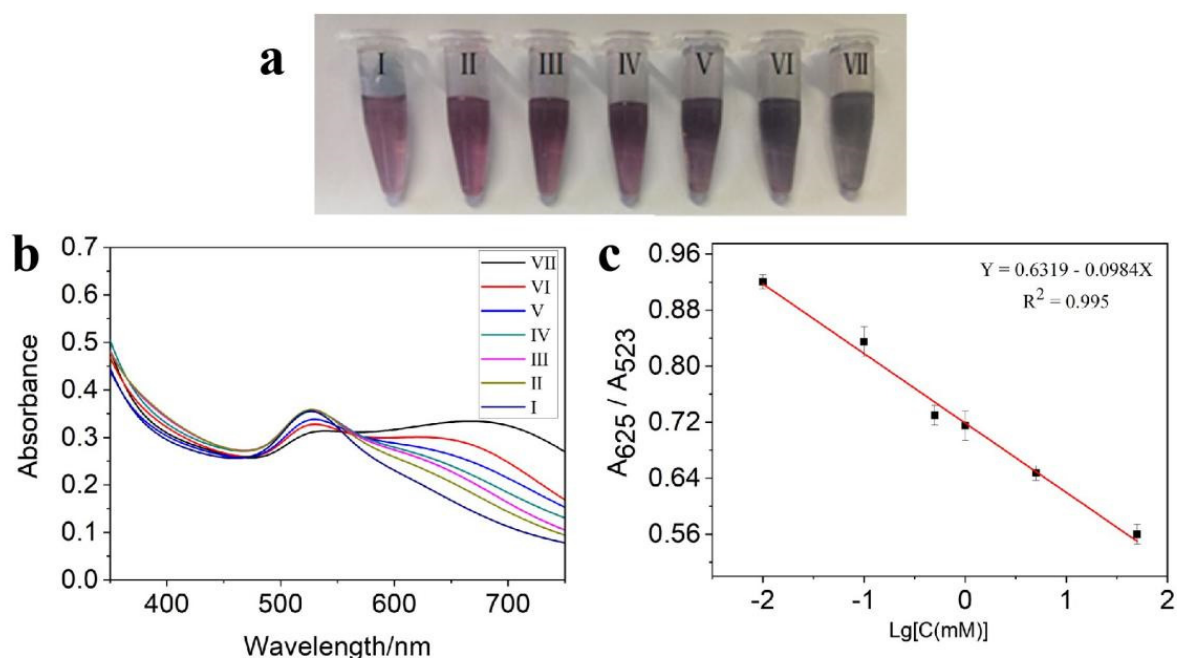

Figure 7. (**a**) Photographs showing the colorimetric detection of glucose with the naked eye: (I) 5 mM, (II) 0.5 mM, (III) 0.1 mM, (IV) 0.05 mM, (V) 0.01 mM, (VI) 0.001 mM, and (VII) 0. (**b**) UV−vis absorption spectra change corresponding with (**a**). (**c**) The linear fitted curve presenting the absorbance ratio of A_{625}/A_{523} at different concentrations of glucose; error bars indicate S (*n* = 3).

Table 2. Comparison of this work with other methods for glucose detection.

Detection Type	Linear Relationship	Liner Range/μM	LOD/μM	Reference
BSA-Cu NCs	-	100–2000	100	[4]
Co_3O_4 NPs	-	-	5	[56]
Pt NPs	-	1–50	1	[57]
Gold films	-	2000–10,000	5	[58]
Ag_2S QDs	$Y = 0.277X + 4.534$ ($R^2 = 0.9945$)	100–12,200	32	[59]
GQDs-AgNPs	$Y = 7.061X + 3.0547$ ($R^2 = 0.9770$)	500–8000	30	[50]
Eu-MOF	$Y = 1.564X + 0.1315$ ($R^2 = 0.9824$)	0.1–4	0.0643	[35]
AuNPs	$Y = 0.6319 - 0.0984X$ ($R^2 = 0.995$)	1–5000	3.01	This work

The specificity of this assay for glucose detection in the HEPES buffer was also evaluated under the same conditions by adding some individual possible interfering species (including sucrose, galactose, and fructose) and their mixture. As illustrated in Figure 8, only glucose can trigger obvious relative absorbance $(I-I_0)/I_0$, and I and I_0 refer to the absorbance ratio of A_{625}/A_{523} of the system with and without glucose, respectively. This demonstrates that the strategy proposed here shows considerable specificity for glucose detection in HEPES buffers.
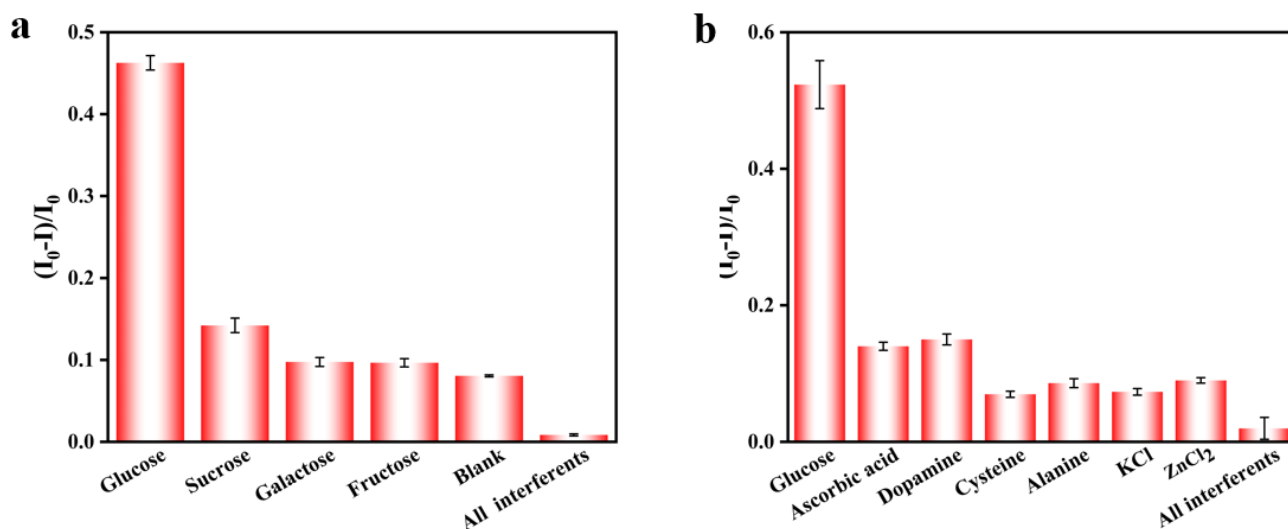
Figure 8. Selectivity of the assay for glucose detection in HEPES buffer (**a**) and diluted serum (**b**).

To test the feasibility of the proposed method, the analysis of glucose in human serum samples was carried out by the standard addition method. The glucose concentration in blood samples measured by a commercial glucose meter is 4.3 ± 0.15 mM. The selectivity of the assay for glucose in diluted serum is shown in Figure 8. The mimetic samples contain the normal diluted serum and different concentrations of glucose. The recoveries range from 81.1% to 118% with the relative standard deviations (RSD) of 1.42%~1.98% (Table 3), indicating the potential applicability of this strategy for glucose detection in diluted human serum samples. RSD is calculated based on the results of three experiments, according to the following equation.

$$\text{RSD} = \frac{S}{\overline{X}} \times 100\% \qquad (1)$$

In Equation (1), S is the standard deviation of found concentrations in the three experiments, and $\overline{X}$ denotes the average value of the found concentration.

Table 3. Detection performance for glucose in healthy human blood serum.

Sample	Spiked Concentration (mM)	Found Concentration (mM)	Recovery (%)	RSD (%)
1	5	4.055	81.1	1.42
2	0.5	0.439	87.8	1.64
3	0.1	0.118	118.0	1.98

4. Conclusions

To summarize, a label-free and visual colorimetric assay was developed for the sensitive detection of H_2O_2 based on the interaction between it and CeO_2. Without H_2O_2, ssDNA decorates the surface of CeO_2 and, almost simultaneously, AuNPs aggregate in the high salt solution. While introducing H_2O_2, it can combine with CeO_2 more firmly. In the presence of H_2O_2, ssDNA bound to CeO_2 is released to bind aggregated AuNPs, causing them to disaggregate, resulting in a purple-to-red color change that can be easily observed by the naked eye. In addition, since H_2O_2 could be generated from the oxidization of glucose by GOx, this strategy could be also utilized to detect glucose even in blood serum samples. Compared with most other methods, this method has higher sensitivity, wider detection range, and lower LOD. This work provides a novel method to monitor H_2O_2 and glucose, which has a promising application in the early diagnosis of some related diseases.

Author Contributions: Conceptualization and writing—original draft, C.Z.; methodology, investigation, and validation, T.W.; methodology, investigation, and validation, J.X.; data analysis and writing—review and editing, D.W.; conceptualization, visualization, supervision, and funding acquisition, L.Y. All authors have read and agreed to the published version of the manuscript.

Institutional Review Board Statement: Not applicable.

Informed Consent Statement: Not applicable.

Data Availability Statement: Not applicable.

Conflicts of Interest: The authors declare no conflict of interest.

References

1. Albers, A.E.; Okreglak, V.S.; Chang, C.J. A FRET-Based approach to ratiometric fluorescence detection of hydrogen peroxide. *J. Am. Chem. Soc.* **2006**, *128*, 9640–9641. [CrossRef] [PubMed]
2. Karyakin, A.A.; Puganova, E.A.; Budashov, I.A.; Kurochkin, I.N.; Karyakina, E.E.; Levchenko, V.A.; Matveyenko, V.N.; Varfolomeyev, S.D. Prussian blue based nanoelectrode arrays for H_2O_2 detection. *Anal. Chem.* **2004**, *76*, 474–478. [CrossRef] [PubMed]
3. Wang, T.; Zhu, H.; Zhuo, J.; Zhu, Z.; Papakonstantinou, P.; Lubarsky, G.; Lin, J.; Li, M. Biosensor based on ultrasmall MoS_2 nanoparticles for electrochemical detection of H_2O_2 released by cells at the nanomolar level. *Anal. Chem.* **2013**, *85*, 10289–10295. [CrossRef] [PubMed]
4. Hua, L.; Yuan, Y.; Zhang, L.; Zhao, J.; Majeed, S.; Xu, G. Copper nanoclusters as peroxidase mimetics and their applications to H_2O_2 and glucose detection. *Anal. Chim. Acta* **2013**, *762*, 83–86. [CrossRef]
5. Chen, S.; Hai, X.; Chen, X.W.; Wang, J.H. In situ growth of silver nanoparticles on graphene quantum dots for ultrasensitive colorimetric detection of H_2O_2 and glucose. *Anal. Chem.* **2014**, *86*, 6689–6694. [CrossRef]
6. Bracamonte, M.V.; Melchionna, M.; Giuliani, A.; Nasi, L.; Tavagnacco, C.; Prato, M.; Fornasiero, P. H_2O_2 sensing enhancement by mutual integration of single walledcarbon nanohorns with metal oxide catalysts: The CeO_2 case. *Sens. Actuators B* **2017**, *239*, 923–932. [CrossRef]
7. Sun, X.; Guo, S.; Liu, Y.; Sun, S. Dumbbell-like PtPd-Fe_3O_4 nanoparticles for enhanced electrochemical detection of H_2O_2. *Nano Lett.* **2012**, *12*, 4859–4863. [CrossRef]
8. Zong, L.; Ruan, L.; Li, J.; Marks, R.S.; Wang, J.; Cosnier, S.; Zhang, X.; Shan, D. Fe-MOGs-based enzyme mimetic and its mediated electrochemiluminescence for in situ detection of H_2O_2 released from Hela cells. *Biosens. Bioelectron.* **2021**, *184*, 113–216. [CrossRef]
9. Xie, B.; Yang, X.; Zhang, R.; Guo, J.; Chen, Z.; He, Y. Hollow and porous Fe_3C-NC nanoballoons nanozymes for cancer cell H_2O_2 detection. *Sens. Actuators B* **2021**, *347*, 130597. [CrossRef]

10. Huo, Y.; Qi, L.; Lv, X.J.; Lai, T.; Zhang, J.; Zhang, Z.Q. A sensitive aptasensor for colorimetric detection of adenosine triphosphate based on the protective effect of ATP-aptamer complexes on unmodified gold nanoparticles. *Biosens. Bioelectron.* **2016**, *78*, 315–320. [CrossRef]

11. Lu, N.; Zhang, M.; Ding, L.; Zheng, J.; Zeng, C.; Wen, Y.; Liu, G.; Aldalbahi, A.; Shi, J.; Song, S.; et al. Yolk–shell nanostructured Fe_3O_4@C magnetic nanoparticles with enhanced peroxidase-like activity for label-free colorimetric detection of H_2O_2 and glucose. *Nanoscale* **2017**, *9*, 4508–4515. [CrossRef] [PubMed]

12. Zhang, R.; Lu, N.; Zhang, J.; Yan, R.; Li, J.; Wang, L.; Wang, N.; Lv, M.; Zhang, M. Ultrasensitive aptamer-based protein assays based on one-dimensional core-shell nanozymes. *Biosens. Bioelectron.* **2020**, *150*, 111881. [CrossRef] [PubMed]

13. Li, J.; Lu, N.; Han, S.; Li, X.; Wang, M.; Cai, M.; Tang, Z.; Zhang, M. Construction of bio-nano interfaces on nanozymes for bioanalysis. *ACS Appl. Mater. Interfaces* **2021**, *13*, 21040–21050. [CrossRef] [PubMed]

14. Guo, Y.; Deng, L.; Li, J.; Guo, S.; Wang, E.; Dong, S. Hemin-graphene hybrid nanosheets with intrinsic peroxidase-like activity for label-free colorimetric detection of single-nucleotide polymorphism. *ACS Nano* **2011**, *5*, 1282–1290. [CrossRef] [PubMed]

15. Dong, Y.; Zhang, H.; Rahman, Z.U.; Su, L.; Chen, X.; Hu, J.; Chen, X. Graphene oxide-Fe_3O_4 magnetic nanocomposites with peroxidase-like activity for colorimetric detection of glucose. *Nanoscale* **2012**, *4*, 3969–3976. [CrossRef] [PubMed]

16. Chen, J.; Jackson, A.A.; Rotello, V.M.; Nugen, S.R. Colorimetric detection of escherichia coli based on the enzyme-induced metallization of gold nanorods. *Small* **2016**, *12*, 2469–2475. [CrossRef]

17. Ju, J.; Zhang, R.; Chen, W. Photochemical deposition of surface-clean silver nanoparticles onnitrogen-doped graphene quantum dots for sensitive colorimetricdetection of glutathione. *Sens. Actuators B* **2016**, *228*, 66–73. [CrossRef]

18. Jin, L.; Meng, Z.; Zhang, Y.; Cai, S.; Zhang, Z.; Li, C.; Shang, L.; Shen, Y. Ultrasmall Pt nanoclusters as robust peroxidase mimics for colorimetric detection of glucose in human serum. *ACS Appl. Mater. Interfaces* **2017**, *9*, 10027–10033. [CrossRef]

19. Zhao, M.; Wang, X.; Ren, S.; Xing, Y.; Wang, J.; Teng, N.; Zhao, D.; Liu, W.; Zhu, D.; Su, S.; et al. Cavity-type DNA origami-based plasmonic nanostructures for raman enhancement. *ACS Appl. Mater. Interfaces* **2017**, *9*, 21942–21948. [CrossRef]

20. Li, H.; Rothberg, L. Colorimetric detection of DNA sequences based on electrostatic interactions with unmodified gold nanoparticles. *Proc. Natl. Acad. Sci. USA* **2004**, *101*, 14036–14039. [CrossRef]

21. Xia, F.; Zuo, X.; Yang, R.; Xiao, Y.; Kang, D.; Bélisle, A.V.; Gong, X.; Yuen, J.D.; Hsu, B.B.; Heeger, A.J.; et al. Colorimetric detection of DNA, small molecules, proteins, and ions using unmodified gold nanoparticles and conjugated polyelectrolytes. *Proc. Natl. Acad. Sci. USA* **2010**, *107*, 10837–10841. [CrossRef] [PubMed]

22. Khavani, M.; Izadyar, M.; Housaindokht, M.R. A combined MD/QM study on the sensing mechanism of Pb^{2+} by glutathione functionalized gold nanoparticles. *J. Mol. Liq.* **2019**, *280*, 120–127. [CrossRef]

23. Jv, Y.; Li, B.; Cao, R. Positively-charged gold nanoparticles as peroxidiase mimic and their application in hydrogen peroxide and glucose detection. *Chem. Commun.* **2010**, *46*, 8017–8019. [CrossRef]

24. Jiang, Y.; Zhao, H.; Lin, Y.; Zhu, N.; Ma, Y.; Mao, L. Colorimetric detection of glucose in rat brain using gold nanoparticles. *Angew. Chem. Int. Ed.* **2010**, *49*, 4800–4804. [CrossRef]

25. Prathap Kumar, M.; Suganya Josephine, G.A.; Sivasamy, A. Oxidation of organic dye using nanocrystalline rare earth metal ion doped CeO_2 under UV and Visible light irradiations. *J. Mol. Liq.* **2017**, *242*, 789–797. [CrossRef]

26. Alhumaimess, M.; Aldosari, O.; Alshammari, H.; Kamel, M.M.; Betiha, M.A.; Hassan, H.M.A. Ionic liquid green synthesis of CeO_2 nanorods and nano-cubes: Investigation of the shape dependent on catalytic performance. *J. Mol. Liq.* **2019**, *279*, 649–656. [CrossRef]

27. Montini, T.; Melchionna, M.; Monai, M.; Fornasiero, P. Fundamentals and catalytic applications of CeO_2-based materials. *Chem. Rev.* **2016**, *116*, 5987–6041. [CrossRef]

28. Yang, S.; Gao, L. Controlled synthesis and self-assembly of CeO_2 Nanocubes. *J. Am. Chem. Soc.* **2006**, *128*, 9330–9331. [CrossRef]

29. Sun, L.; Ding, Y.; Jiang, Y.; Liu, Q. Montmorillonite-loaded ceria nanocomposites with superiorperoxidase-like activity for rapid colorimetric detection of H_2O_2. *Sens. Actuators B* **2017**, *239*, 848–856. [CrossRef]

30. Liu, Q.; Yang, Y.; Lv, X.; Ding, Y.; Zhang, Y.; Jing, J.; Xu, C. One-step synthesis of uniform nanoparticles of porphyrinfunctionalized ceria with promising peroxidase mimetics for H_2O_2 and glucose colorimetric detection. *Sens. Actuators B* **2017**, *240*, 726–734. [CrossRef]

31. Devaiah, D.; Reddy, L.H.; Park, S.; Reddy, B.M. Ceria–zirconia mixed oxides: Synthetic methods and applications. *Catal. Rev.* **2018**, *60*, 177–277. [CrossRef]

32. Liu, B.; Sun, Z.; Huang, P.J.; Liu, J. Hydrogen peroxide displacing DNA from nanoceria: Mechanism and detection of glucose in serum. *J. Am. Chem. Soc.* **2015**, *137*, 1290–1295. [CrossRef] [PubMed]

33. Chen, S.; Zheng, H.; Wang, J.; Hou, J.; He, Q.; Liu, H.; Xiong, C.; Kong, X.; Nie, Z. Carbon nanodots as a matrix for the analysis of low-molecularweight molecules in both positive- and negative-ion matrix-assisted laser desorption/ionization time-of-flight mass spectrometry and quantification of glucose and uric acid in real samples. *Anal. Chem.* **2013**, *85*, 6646–6652. [CrossRef] [PubMed]

34. Yuan, J.; Cen, Y.; Kong, X.J.; Wu, S.; Liu, C.L.; Yu, R.Q.; Chu, X. MnO_2-nanosheet-modified upconversion nanosystem for sensitive turn-on fluorescence detection of H_2O_2 and glucose in blood. *ACS Appl. Mater. Interfaces* **2015**, *7*, 10548–10555. [CrossRef]

35. Cui, Y.; Chen, F.; Yin, X. A ratiometric fluorescence platform based on boric-acid-functional Eu-MOF for sensitive detection of H_2O_2 and glucose. *Biosens. Bioelectron.* **2019**, *135*, 208–215. [CrossRef]

36. Adeel, M.; Asif, K.; Rahman, M.M.; Daniele, S.; Canzonieri, V.; Rizzolio, F. Glucose detection devices and methods based on metal–organic frameworks and related materials. *Adv. Funct. Mater.* **2021**, *31*, 2106023. [CrossRef]

37. Sun, Q.; Liu, Q.; Gao, W.; Xing, C.; Shen, J.; Liu, X.; Kong, X.; Li, X.; Zhang, Y.; Chen, Y. A high-performance photoelectrochemical sensor for the specific detection of H_2O_2 and glucose based on an organic conjugated microporous polymer. *J. Mater. Chem. A* **2021**, *9*, 26216–26225. [CrossRef]

38. Liang, T.; Zou, L.; Guo, X.; Ma, X.; Zhang, C.; Zou, Z.; Zhang, Y.; Hu, F.; Lu, Z.; Tang, K.; et al. Rising mesopores to realize direct electrochemistry of glucose oxidase toward highly sensitive detection of glucose. *Adv. Funct. Mater.* **2019**, *29*, 1903026. [CrossRef]

39. Liu, B.; Liu, J. Comprehensive screen of metal oxide nanoparticles for DNA adsorption, fluorescence quenching, and anion discrimination. *ACS Appl. Mater. Interfaces* **2015**, *7*, 24833–24838. [CrossRef]

40. Xua, M.; Gao, Z.; Zhou, Q.; Lin, Y.; Lu, M.; Tang, D. Terbium ion-coordinated carbon dots for fluorescent aptasensing of adenosine 5′-triphosphate with unmodified gold nanoparticles. *Biosens. Bioelectron.* **2016**, *86*, 978–984. [CrossRef]

41. Liu, P.; Yang, X.; Wang, Q.; Wang, K. Enzyme-free colorimetric detection of DNA by using gold nanoparticles and hybridization chain reaction amplification. *Anal. Chem.* **2013**, *85*, 7689–7695. [CrossRef] [PubMed]

42. Chen, H.; Zhang, J.; Wu, H.; Koh, K.; Yin, Y. Sensitive colorimetric assays for a-glucosidase activity and inhibitor screening based on unmodified gold nanoparticles. *Anal. Chim. Acta* **2015**, *875*, 92–98. [CrossRef] [PubMed]

43. Ramezani, M.; Danesh, N.M.; Abnous, P.L.; Taghdisi, S.M. A selective and sensitive fluorescent aptasensor for detection of kanamycin based on catalytic recycling activity of exonuclease III and gold nanoparticles. *Sens. Actuators* **2016**, *222*, 1–7. [CrossRef]

44. Haiss, W.; Thanh, N.T.; Aveyard, J.; Fernig, D.G. Determination of size and concentration of gold nanoparticles from UV-vis spectra. *Anal. Chem.* **2007**, *79*, 4215–4221. [CrossRef] [PubMed]

45. Azmi, N.E.; Ramli, N.I.; Abdullah, J.; Hamid, M.A.; Sidek, H.; Rahman, S.A.; Ariffin, N.; Yuso, N.A. A simple and sensitive fluorescence based biosensor for the determination of uric acid using H_2O_2-sensitive quantum dots/dual enzymes. *Biosens. Bioelectron.* **2015**, *67*, 129–133. [CrossRef] [PubMed]

46. Liu, X.; Atwater, M.; Wang, J.; Huo, Q. Extinction coefficient of gold nanoparticles with different sizes and different capping ligands. *Colloids Surf. B* **2007**, *58*, 3–7. [CrossRef] [PubMed]

47. Lv, L.; Jin, Y.; Kang, X.; Zhao, Y.; Cui, C.; Guo, Z. PVP-coated gold nanoparticles for the selective determination of ochratoxin a via quenching fluorescence of the free aptamer. *Food Chem.* **2018**, *249*, 45–50. [CrossRef]

48. Wang, L.; Cao, H.X.; Pan, C.G.; He, Y.S.; Liu, H.F.; Zhou, L.H.; Li, C.Q.; Liang, G.X. A fluorometric aptasensor for bisphenol a based on the inner filter effect of gold nanoparticles on the fluorescence of nitrogen-doped carbon dots. *Microchim. Acta* **2019**, *28*, 186. [CrossRef]

49. Teodoroa, K.B.R.; Migliorini, F.L.; Christinelli, W.A.; Correa, D.S. Detection of hydrogen peroxide (H_2O_2) using a colorimetric sensor based on cellulose nanowhiskers and silver nanoparticles. *Carbohydr. Polym.* **2019**, *212*, 235–241. [CrossRef]

50. Nguyen, N.D.; Nguyen, T.V.; Chu, A.D.; Tran, H.V.; Tran, L.T.; Huynh, C.D. A label-free colorimetric sensor based on silver nanoparticles directed to hydrogen peroxide and glucose. *Arab. J. Chem.* **2018**, *11*, 1134–1143. [CrossRef]

51. Luo, Y.; Liu, H.; Rui, Q.; Tian, Y. Detection of extracellular H_2O_2 released from human liver cancer cells based on TiO_2 nanoneedles with enhanced electron transfer of cytochromec. *Anal. Chem.* **2009**, *81*, 3035–3041. [CrossRef] [PubMed]

52. Wang, H.; Bo, X.; Bai, J.; Wang, L.; Guo, L. Electrochemical applications of platinum–palladium alloy nanoparticles/large mesoporous carbon. *J. Electroanal. Chem.* **2011**, *662*, 281–287. [CrossRef]

53. Kang, X.; Wang, J.; Tang, Z.; Wu, H.; Lin, Y. Direct electrochemistry and electrocatalysis of horseradish peroxidase immobilized in hybrid organic–inorganic film of chitosan/sol–gel/carbon nanotubes. *Talanta* **2009**, *78*, 120–125. [CrossRef] [PubMed]

54. Zhao, X.; Mai, Z.; Kang, X.; Zou, X. Direct electrochemistry and electrocatalysis of horseradish peroxidase based on clay–chitosan-gold nanoparticle nanocomposite. *Biosens. Bioelectron.* **2008**, *23*, 1032–1038. [CrossRef] [PubMed]

55. Xiao, F.; Li, Y.; Zan, X.; Liao, K.; Xu, R.; Duan, H. Growth of metal–metal oxide nanostructures on freestanding graphene paper for flexible biosensors. *Adv. Funct. Mater.* **2012**, *22*, 2487–2494. [CrossRef]

56. Mu, J.; Wang, Y.; Zhao, M.; Zhang, L. Intrinsic peroxidase-like activity and catalase-like activity of Co_3O_4 nanoparticles. *Chem. Commun.* **2012**, *48*, 2540–2542. [CrossRef]

57. Ju, Y.; Kim, J. Dendrimer-encapsulated Pt nanoparticles with peroxidase-mimetic activity as biocatalytic labels for sensitive colorimetric analyses. *Chem. Commun.* **2015**, *51*, 13752–13755. [CrossRef]

58. Li, Y.; Song, Y.Y.; Yang, C.; Xia, X.H. Hydrogen bubble dynamic template synthesis of porous gold for nonenzymatic electrochemical detection of glucose. *Electrochem. Commun.* **2007**, *9*, 981–988. [CrossRef]

59. Zhang, X.; Liu, M.; Liu, H.; Zhang, S. Low-toxic Ag_2S quantum dots for photoelectrochemical detection glucose and cancer cells. *Biosens. Bioelectron.* **2014**, *56*, 307–312. [CrossRef]